A parametric study to simulate the non-Newtonian turbulent flow in spiral tubes

Valizadeh, Kamran; Farahbakhsh, Soroush; Bateni, Amir; Zargarian, Amirhossein; Davarpanah, Afshin; Alizadeh, Araz; Zarei, Mojtaba

Published in:
Energy Science and Engineering

DOI:
10.1002/ese3.514

Publication date:
2020

Citation for published version (APA):
Valizadeh, K., Farahbakhsh, S., Bateni, A., Zargarian, A., Davarpanah, A., Alizadeh, A., & Zarei, M. (2020). A parametric study to simulate the non-Newtonian turbulent flow in spiral tubes. *Energy Science and Engineering*, *8*(1), 134-149. https://doi.org/10.1002/ese3.514

Received: 18 July 2019 | Revised: 30 August 2019 | Accepted: 25 September 2019

DOI: 10.1002/ese3.514

RESEARCH ARTICLE

Energy Science & Engineering Open Access

A parametric study to simulate the non-Newtonian turbulent flow in spiral tubes

Kamran Valizadeh[1] | **Soroush Farahbakhsh**[2] | **Amir Bateni**[3] | **Amirhossein Zargarian**[4] | **Afshin Davarpanah**[5,6] | **Araz Alizadeh**[7] | **Mojtaba Zarei**[8]

[1]Department of Chemical Engineering, Science and Research Branch, Islamic Azad University, Tehran, Iran

[2]Department of Mechanical Engineering, K. N. Toosi University of Technology, Tehran, Iran

[3]Department of Chemical Engineering, Arak Branch, Islamic Azad University, Arak, Iran

[4]School of Engineering, University of South Australia, Mawson Lakes, SA, Australia

[5]Department of Petroleum Engineering, Science and Research Branch, Islamic Azad University, Tehran, Iran

[6]Department of Mathematics, Aberystwyth University, Ceredigion, Wales, UK

[7]Department of Natural Resources and Environment, Science and Research Branch, Islamic Azad University, Tehran, Iran

[8]Department of Chemical Engineering, Shahreza Branch, Islamic Azad University, Shahreza, Iran

Correspondence
Afshin Davarpanah, Department of Mathematics, Aberystwyth University, Ceredigion SY23 3BZ, Wales, UK.
Email: Afd6@aber.ac.uk

Abstract

Non-Newtonian fluids are considered to those types of fluids that do not follow Newton's law of viscosity where viscosity would change in either more solid or liquid. The objective of this study, a parametric simulation, was performed to investigate the considerable influence of non-Newtonian fluids on different parameters on spiral tubes. Firstly, governing equations have derived by computational fluid dynamics methods to compare the laminar and turbulent flows. Then, the turbulent flow, the non-Newtonian flow, power law flow, and cross models are simulated according to the boundary conditions. Consequently, for the Reynolds range of 600-2500, increasing the Reynolds number decreases the friction coefficient. It is observed that in slow flow, there is no significant difference between the results of cross and power law models. The distribution of velocity profile has slight variation at the pipe outlet for Reynolds 9000 and 20 000. In other words, the flow is constant in developed region inside the spiral pipe. Moreover, the investigation of pressure drop inside the pipe revealed that regarding the increase in Reynolds number, the friction coefficient decreases. In spiral tubes, due to the presence of secondary currents, the friction coefficient is higher than the direct tube.

KEYWORDS

computational fluid dynamics, governing equations, non-Newtonian flow, Reynolds number, turbulent flow

1 | INTRODUCTION

One of the ways to improve heat transfer efficiency is to use a spiral structure for tubes instead of conventional direct tubes. Compared to the direct tubes, spiral tubes have a more compact surface and have higher heat transfer and friction coefficients. When the fluid flows through the spiral tubes, it influences by the centrifugal force which this centrifugal force creates a secondary flow in the fluid, and as a result, this secondary flow increases the axial flow velocity near the outer wall of the tube. Thereby increasing the axial velocity will reduce the thermal resistance and

thereby increase the heat transfer coefficient. Moreover, increasing the velocity will increase the friction coefficient and, as a result, increase the pressure drop of the fluid in the direct tubes. In the spiral tubes, the factors that affected heat transfer coefficient and pressure drop include the Reynolds number, Prandtl number, Newtonian or non-Newtonian of the fluid, and well boundary conditions which are depended to the tube radius, coil radius, and coil steps. Due to the compact structure and the high coefficient of heat transfer in the coils, spiral tube of heat exchangers is used in a variety of industries such as cryogenic industries, natural gas liquefaction, food and pharmaceutical industries, refrigeration, and air conditioning.[1-5]

Different non-Newtonian fluids such as polyox and clay suspensions have been used in numerous industries. Regarding the complexity of flow behavior of non-Newtonian fluids in spiral tubes or coiled pipes, it is necessary to rearrange the derived formulas according to the characteristics of these fluids.[6-11] Regarding the produced secondary fluid flow that is made by centrifugal forces in spiral tubes, the components of velocity are made in the existed directions. In the upcoming years, numerous studies and analytical investigations have been performed in curved tubes (spiral tubes or coiled pipes).[12-16] According to Dean's study, the gradient of pressure drop is depended to the curvature of the spiral tube in curved pipes and tubes. Spiral tubes are of great importance in terms of geometry and heat transfer efficiency.[17-19] These types of converters can be found in energy recovery systems, nuclear reactors, and medical devices such as dialysis and many other applications.[20-23] One of the essential advantages of using spiral tubes as heat exchangers is their higher adequate level than direct tubes in the same volume. In other words, these pipes can accommodate a significant exchange of heat in a small space.[24,25] In 1967, the internal and external heat transfer coefficients of the thermal system including spiral tubes were studied in a stirrer vessel. They proposed five different tubes were considered at different velocities and operational conditions. They provided an equation for calculating the Nusselt number based on the spiral tube geometry.[26] Jones et al[27] proposed a method to increase efficiency and increase turbulence without using a stirrer. In this method, different diameters were used for spiral pipes.[27] They explored the impact of this geometry on the spiral tube heat transfer coefficient inspired by the study of Jones et al,[27] and they proposed geometry for spiral tubes. They investigated two experimental correlations for the Nusselt number in terms of the curvature coefficients of the spiral tube and the Reynolds and Prandtl numbers for two intervals of material with a Prandtl higher than one and a Prandtl number smaller than one.[26] In 1997, the coefficient of external surface heat transfer for spiral tubes was also achieved.[28] The heat transfer coefficient of the tubes was obtained by Kalb and Seader[29] by providing an empirical correlation.[29] Due to the lack of cheap and fast processor systems, no numerical studies were conducted on spiral tubes until 1995, and simulated these tubes in a comprehensive and valuable study, and examined the effect of the Prandtl number and the spiral curve step on these tubes.

Regarding the required simplifications of non-Newtonian fluids in curved pipes, several analytical models were proposed by researchers; however, these estimations would not agree with the experimental results of Rajasekaran et al[30] that they found that rheological properties and the curvature of these fluids proportionally influence the pressure drop in every dimension. Firstly, the value of pressure drop in the diameter axis would explicitly be depicted that the secondary flow is the function of curvature ratio. Even though Raju and Ratna[31] proposed theoretical predictions of non-Newtonian fluid, the considerable influence of curvature ratio on the heat transfer and momentum in spiral tubes were not in the excellent agreement with experiment results.[31] Nakayama et al[32] investigated numerically in a helix tubing system.[32] Jayakumar et al[33] studied the heat transfer of heat exchangers for shell and tubes with spiral tubes using FLUENT software, and the purpose of this study was to obtain a Nusselt number and compulsory displacement of the inner surface of the tube.[33] In 2010, Jayakumar et al[34] analyzed the single-phase CFD flow into spiral tubes.[34-37]

Although there are numerous studies have reported in the literature to investigate the considerable influence of non-Newtonian fluids in heat exchangers, in this comprehensive study, the dynamical behavior of non-Newtonian fluids in the turbulent flow of spiral tubes has been proposed, and various models of turbulence, instability, roughness, and heat transfer in these tubes were performed. Furthermore, the Newtonian, Power low, and Cross models were simulated using ANSYS and FLUENT software. The effect of Reynolds number on the friction coefficient inside the spiral tube and shear stress on the wall, the impact of n and K on the friction coefficient and pressure drop, and the effect of roughness in turbulent flow on heat transfer enhancement and friction coefficient were carried out. On the other hand, heat transfer characteristics in constant temperature and constant thermal flux were considered in this study. Subsequently, there are plenty of correlations with non-Newtonian flows; they are all within a specific range of conditions and cannot be generalized to all models. Thereby, the use of experimental models requires a lot of time and vast expenditures. To reduce these costs and modeling in the shortest possible time, using numerical methods by commercial software or programming can be partly responsible for these constraints. However, it is still not possible to rely on these new methods due to hardware and software limitations.

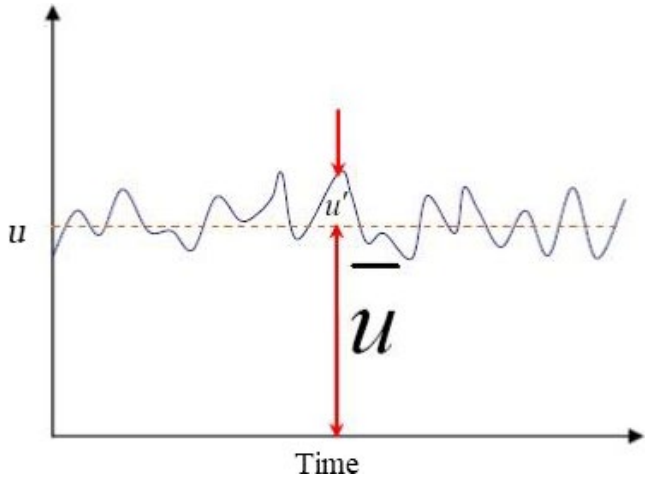

FIGURE 1 Velocity changes vs time in one point of turbulent flow

2 | GOVERNING EQUATIONS

In this part of the study, the turbulent flows and their governing equations were derived, and the various models proposed for numerical solution of the turbulent flows. In the following, the generalization method of these equations is presented for non-Newtonian flows and their differences with Newtonian flows, as well as the way of discretization and the required assumptions for these models to be used.

2.1 | A statistical method to investigate turbulent flows

If a specific point is considered in the flow field within a pipe, and its velocity is calculated in terms of time, the curve is similar to Figure 1 (FLUENT)[38].

As can be seen in Figure 1, the turbulent velocity field $u(t)$ is obtained by the combination of two parts of mean velocity $\overline{u}$ and fluctuating velocity u, which is defined as the velocity fluctuation during the time.

$$u(t)=\overline{u}^{\text{steady}}_{\text{value}}+u'(t)^{\text{fluctuating}}_{\text{component}} \tag{1}$$

The average velocity is defined as follows:

$$\overline{u}=\frac{1}{T_1}\int_0^{T_1} dt \tag{2}$$

where T_1 is chosen so large that in the case of time values larger than T_1, no change is observed in the integral size. In other words, $\overline{u}$ must be independent of the selected time T_1. The loading symbol (-) on the velocity component represents the average time quantity, and u is the vacillation velocity component. In general, the mean quantity $\overline{\eta}$ can be calculated in two ways: ensemble averaging and time averaging.

2.2 | Continuity equation for turbulent flows

The differential form of the continuity equation is as follows:

$$\frac{\partial\rho}{\partial t}+\frac{\partial}{\partial x_i}(\rho u_i)=0 \tag{3}$$

In general, the conservation equations governing the turbulent fluid flow can be written as follows:

2.2.1 | Momentum conservation

$$\rho\left[\frac{\partial u_i}{\partial t}+u_j u_{i,j}\right]=-P_i+(\rho-\rho_0)g_i+\left[\mu(u_{i,j}+u_{j,i})-\rho\overline{u_i'u_j'}\right]_j \tag{4}$$

2.2.2 | Energy conservation

$$\rho C_p\left[\frac{\partial T}{\partial t}+u_j T_j\right]=(\lambda T_j-\rho C_p\overline{u_j'T'})_j+H \tag{5}$$

The parameter λ in the above equation expresses the thermal conductivity. The above equations are called RANS equations. These formulas are explicit that no assumptions have been made to obtain them or to simplify them.

2.3 | Turbulence energy equation in turbulent flows

If the momentum equation was used for incompressible flow with a static viscosity, the following equation would be obtained by multiplication of the velocity component along the i in momentum equation, and then, it is simplified as follows:

$$\frac{\partial}{\partial t}\left(\frac{u_i u_j}{2}\right)=-\frac{\partial}{\partial x_i}\left[u_i\left(\frac{p}{\rho}+\frac{u_i u_j}{2}\right)\right]+\nu\frac{\partial}{\partial x_j}\left[u_i\left(\frac{\partial u_i}{\partial x_j}+\frac{\partial u_j}{\partial x_i}\right)\right]-\nu\left(\frac{\partial u_i}{\partial x_j}+\frac{\partial u_j}{\partial x_i}\right)\frac{\partial u_i}{\partial x_j} \tag{6}$$

The above equation has an energy unit and is called "energy equation." The following equations were extracted from Equation 6. $(\rho\overline{u_i'u_j'})$ is defined as the mean of density-weighted fluctuation, and $\tau_{ij,\text{Turb}}$ is the Reynolds stress tensor.

$$\tau_{ij}=\mu\left(\frac{\partial\overline{u}_i}{\partial x_j}+\frac{\partial\overline{u}_j}{\partial x_i}\right)-\rho\overline{u_i'u_j'}=\tau_{ij,\text{Lam}}+\tau_{ij,\text{Turb}} \tag{7}$$

$$\tau_{ij,\text{Lam}}=\mu\left(\frac{\partial\overline{u}_i}{\partial x_j}+\frac{\partial\overline{u}_j}{\partial x_i}\right) \tag{8}$$

$$\tau_{ij,\text{Turb}} = -\rho\overline{u_i' u_j'} \tag{9}$$

2.4 | Wall boundary condition

The wall boundary condition is used on the boundaries in which the fluid is enclosed by a solid. In viscous flows, being not viscosity for flow which is sticking to the wall is assumed to be on FLUENT software. The flow velocity, which is sticking to the wall, can be determined by calculating the shear stress value. The FLUENT software uses flow characteristics in adjacent wall elements for viscous flow simulation to calculate and predict the shear stress value. In slow flows, shear stress calculation depends only on the velocity gradient on the boundary of the wall. In slow flows, shear stress of the wall is obtained in terms of the vertical velocity gradient ratio to the wall (Equation 10). If the vertical velocity gradient ratio to the wall is high, it is necessary that the network which is close to the wall border is sufficiently excellent so that it can cover appropriately the flow changes within the boundary layer.

$$\tau_w = \mu \frac{\partial v}{\partial y} \tag{10}$$

3 | RESULTS AND DISCUSSIONS

The purpose of this comprehensive study is to investigate the flow and the heat transmission of non-Newtonian fluids in a spiral pipe and to compare their results with Newtonian fluid flow regarding the specific characteristics of non-Newtonian fluids especially viscosity alteration by using the $k-w$ model. Then, by using FLUENT software, a spiral pipe with the features that are statistically given in Table 1 were simulated in the Reynolds ranges of 2000-20000 for turbulent flow regimes to compare with the empirical results.. Finally, we choose an appropriate turbulent model.

3.1 | Geometry draw

Gambit 2.4 software is used to draw spiral coils and networking them. The flow is not developed at the beginning of the pipe. As the effects of undeveloped flow are reduced on final results, the flow has been used in a two-step pipe.

TABLE 1 The geometric properties of the coil

	Coil diameter (D_c) mm	Pipe diameter (d) mm	Coil height (H) mm
Coil no. 1	274.6	20.8	29.15

The schematic geometry of spiral tubes which is plotted by Gambit software is shown in Figure 2.

3.2 | Numerical solution by FLUENT software and network selection

When it comes to turbulence in non-Newtonian fluids, there is no physically consistent turbulence model yet. What FLUENT does, is replacing the molecular viscosity with the apparent one in the RANS equations. In FLUENT software, Green-Gouss cell-based discretization is based on pressure to solve the equations. The turbulence $k-\varepsilon$ model is considered for modeling the turbulent effects. The gravity effect was also discussed. The velocity and coil pressure equations are solved by SIMPLEC algorithm. The momentum equations and volume fractions were used with the accuracy of the QUICK scheme, and the power law scheme was used for turbulent kinetic energy generation rate and dispersion coefficient. The convergence criterion was equal to 10^{-6} for velocity, continuity, and volume fraction equations. According to the output-velocity distribution graph Figure 3, it is observed that there is no difference between the results of networks B (160 992) and C (239 104). Therefore, we choose network B as an appropriate network. It should be noted that by increasing Reynolds number, the network becomes finer. In the following Figure, the network used is shown for Reynolds number 19 000. To assess the independence of the solution from the network, geometry with the following characteristics is used. For non-Newtonian fluid, the parameters of mean quality, temperature dependency, types of model, and flow regimes (laminar or turbulent) should be considered in simulation procedures, while for Newtonian fluids, only

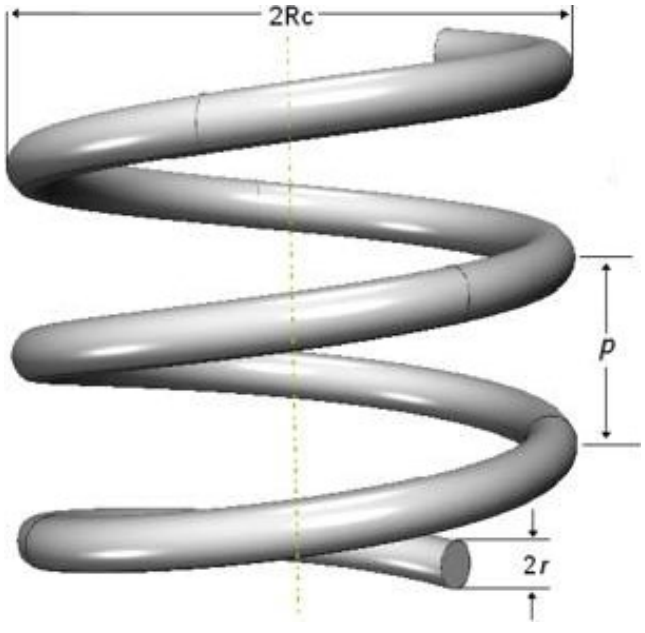

FIGURE 2 The geometry of the spiral coil

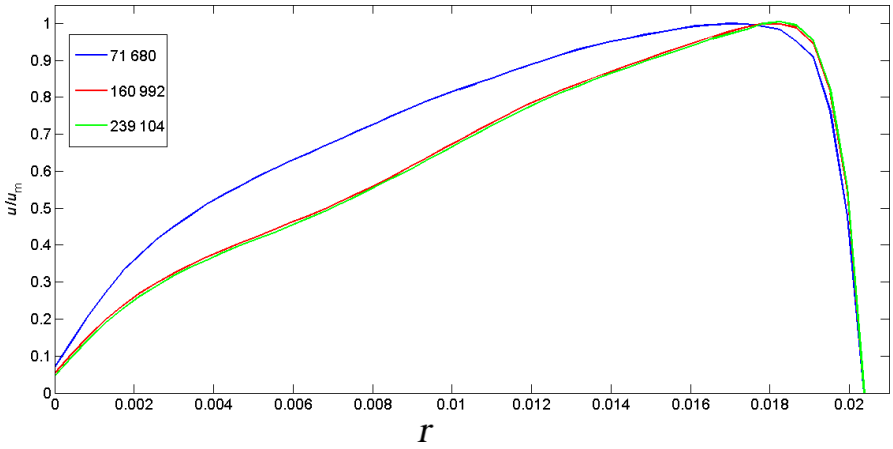

FIGURE 3 The velocity profile in the outlet

velocity is considered as the crucial parameters in the simulation procedures.

The boundary conditions, which is considered in this simulation, are statistically considered Table 2.

3.3 | Verification of Results

To verify the accuracy of the results, they are compared according to Pawar and Sunnapwar[39] for 10% glycol, thermal flux 50.000 W/m^2, and the input temperature of 375 K for different Reynolds numbers using various turbulent models.[39]

As shown in Figure 4, the practical and numerical results are very close for Reynolds numbers higher than 9000 and the lower Reynolds, the more differences between empirical and numerical results because the flow is getting closer to the transition condition. For Newtonian and non-Newtonian fluids, the results for friction coefficient are compared with the empirical relations,[40] as well as the results of Srinivasan et al[41] in Figure 5. As shown in Figure 5, for Reynolds numbers higher than 10 000, the results of numerical and empirical solutions are close.[41] However, for Reynolds numbers less than 10 000, the difference between such results increases due to get closer to the transition condition. The flow is very unstable at transition condition and that is why the empirical results may differ in this zone. This is obvious in Figure 5 that the difference in results has been increased in Reynolds numbers which are close to the transition state.

3.4 | Different model assessment

3.4.1 | Slow flow

To investigate the slow flow, we categorize the fluid into three Newtonian, power law, and cross models, and the flow is solved by FLUENT software for the Reynolds range of 600-2500. As can be seen in Figure 6, the more increase in Reynolds number is caused by the less friction coefficient. In the slow flow, the non-Newtonian model is solved with n = 0.75, and the friction coefficient value is lower than the

TABLE 2 Boundary conditions

Parameter	Value
Consistency index	0.044
Power law index	0.75
Reference temperature	0
Minimum viscosity limit	0.0001
Maximum viscosity limit	1000
Inlet velocity	1 m/s
Convergence time	5 h

corresponding value for Newtonian fluid. In the slow flow, there are not any significant differences between the results of cross and power law models. As it is evident in Figure 7, the pressure drop also increases when the Reynolds number increases, however, the friction coefficient increases. The effect of velocity increase will overcome the impact of decreasing friction coefficient and will increase the pressure drop and shear stress because shear stress and pressure drop are proportional to the velocity squared. It is schematically depicted in Figure 8. As Reynolds increases near the wall, the velocity gradient rises, and it will increase the shear stress of the wall. However, the friction coefficient has a negative relationship with velocity squared, the effect of increasing the velocity in $f = \frac{\tau}{\frac{1}{2}\rho V^2}$ will overcome the shear stress increasing, and it will decrease the friction coefficient. It is plotted in Figure 9.

3.5 | Investigating the flow consistency

The turbulent flows are inherently unstable, but in the cases that the unstable flow is stable, it can be solved as a stable one. The unbalanced system is a system in which the physical component distribution of the flow changes with small turbulence. The flow in the inlet region of the pipe is an example of an unstable flow. In the present work, we calculate the distribution of velocity profile for two different

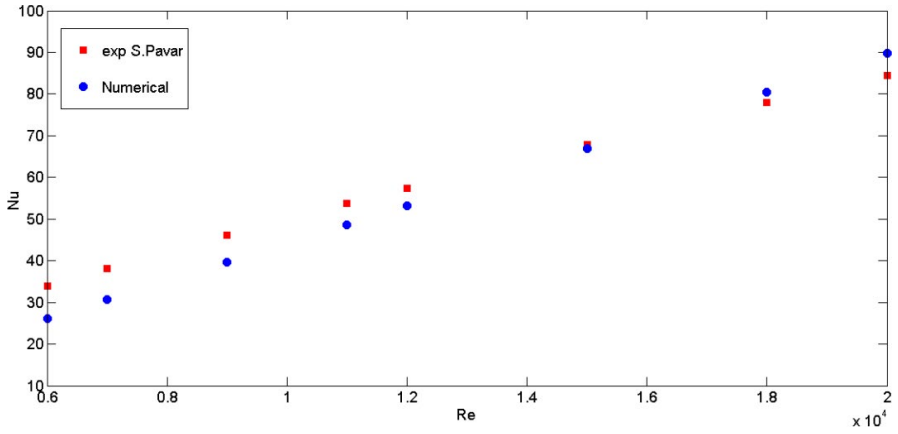

FIGURE 4 Comparison of the results of the numerical solution and empirical values[39]

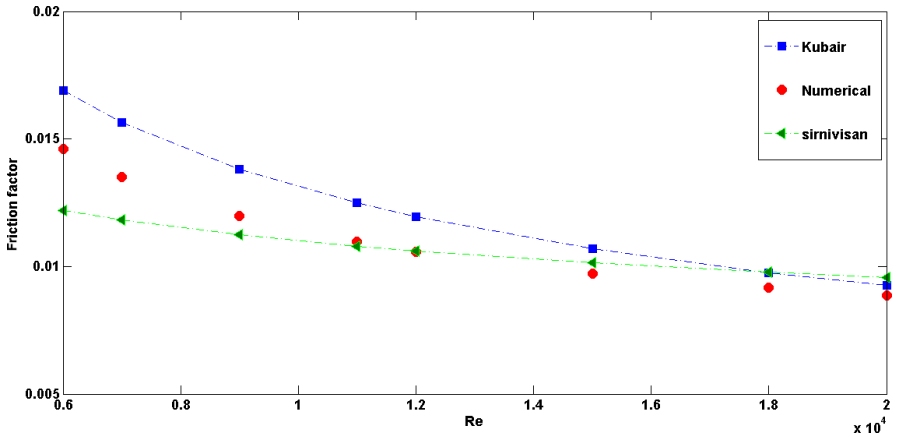

FIGURE 5 Comparison of numerical solution and empirical relation results

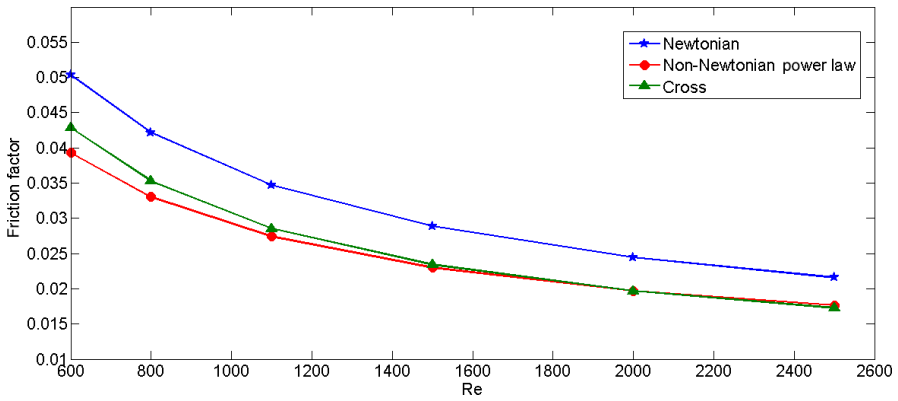

FIGURE 6 Friction factor for different Reynolds numbers in the laminar flow

velocities to assess the stability of the flow inside the spiral pipe. As shown in Figure 10, the distribution of velocity profile at the pipe outlet for two Reynolds numbers 9000 and 20 000 has an insignificant difference, so it can be said that the flow is stable in the developed region inside the spiral pipe.

3.5.1 | Turbulent flow

As can be seen in Figure 11, the turbulent flow was solved by FLUENT software for k-e and k-w turbulence models, and the results of the k-w model are more consistent with experimental results. That is why the k-w model was used to examine the various parameters in a turbulent flow.

The Newtonian, power law, and cross models were simulated by FLUENT software to examine the turbulent flow. In Figure 12, the effect of increasing Reynolds number is shown on the friction coefficient inside the spiral pipe. As seen, the more Reynolds number, the less the friction coefficient is. The amount of friction coefficient in spiral pipes is greater than in the direct pipes, due to the secondary flows.

In Figure 13, the pressure drop inside the pipe is plotted in terms of various Reynolds numbers. Although the friction coefficient decreases by increasing in Reynolds number, the

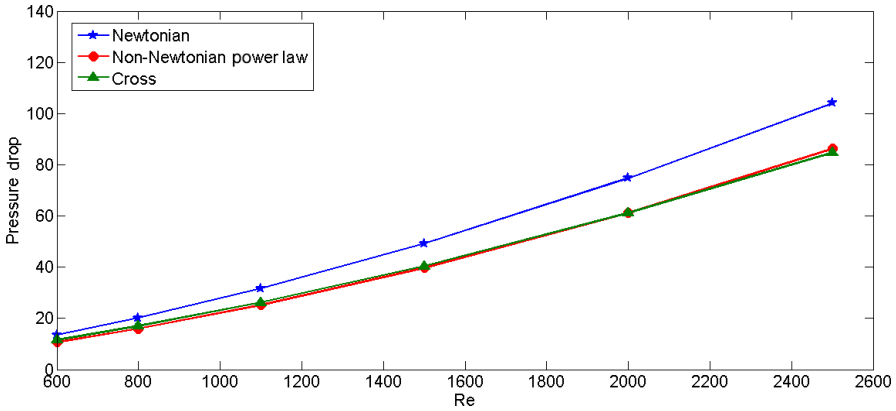

FIGURE 7 Pressure drop for laminar flow in different Reynolds

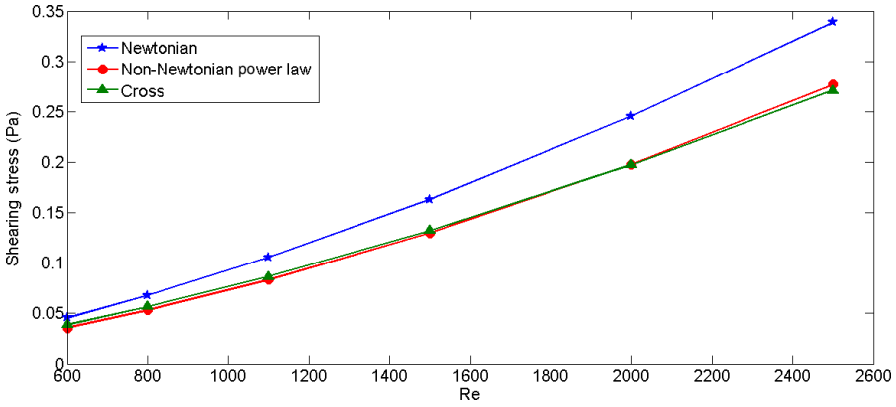

FIGURE 8 Shear stress for laminar flow in different Reynolds

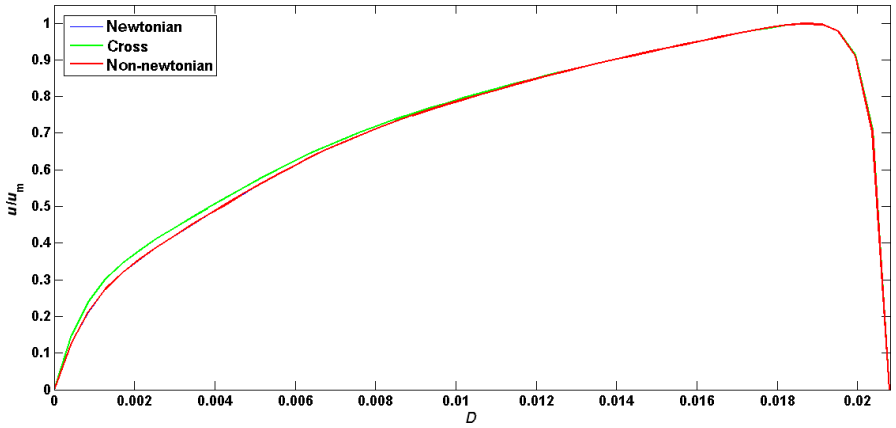

FIGURE 9 Velocity distribution in the outlet for different models with n = 0.75

increase in turbulence of the flow inside the pipe causes an increase in the pressure drop in the pipe.

In the flow inside the pipe, increasing in Reynolds number decreases the thickness of the boundary layer and increases the velocity gradient within the boundary layer, and according to $\tau = \mu_0 \left(\frac{\partial u}{\partial n}\right)$, increasing in velocity gradient will increase the shear stress of the wall, which is shown in Figure 14.

In the flow inside the spiral pipe, due to the centrifugal force and the higher radius near the outlet surface, the velocity increases as it moves away from the coil center, and this causes that the shear stress in the outer wall is higher than the shear stress in the inner wall of the coil. The velocity contours clearly show the effect of coil curvature on the shear stress, and we can conclude the dependence of shear stress on the coil curvature. By decreasing the coil curvature, velocity gradient increases on the central line of the cross section, which is shown in Figure 15.

3.6 | The geometry effect

As shown in Figure 16, changing in the coil curve $\left(\text{delta} = {}^{d}/_{D_c}\right)$ has a significant effect on the pressure drop, where d is the pipe diameter and D_c is the coil diameter. As the coil curve increases (decreasing diameter), centrifugal force

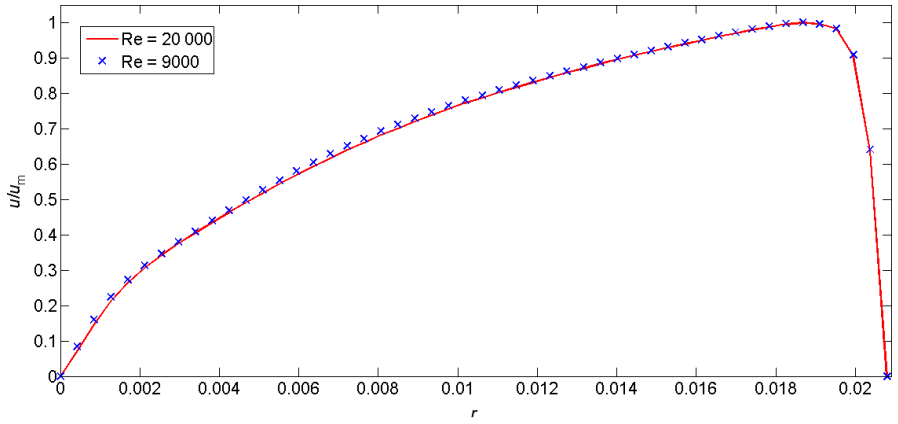

FIGURE 10 Dimensionless velocity distribution for Reynolds number of 9000 and 20 000

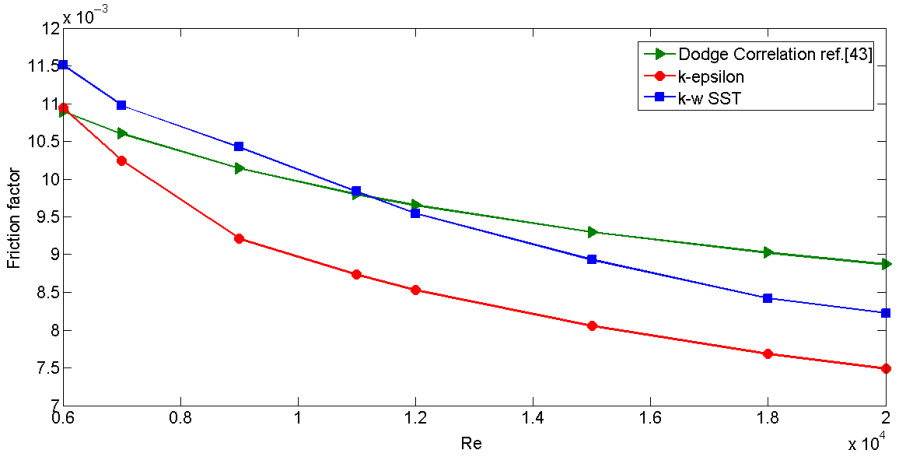

FIGURE 11 Comparison of turbulent models for k-w and k-epsilon

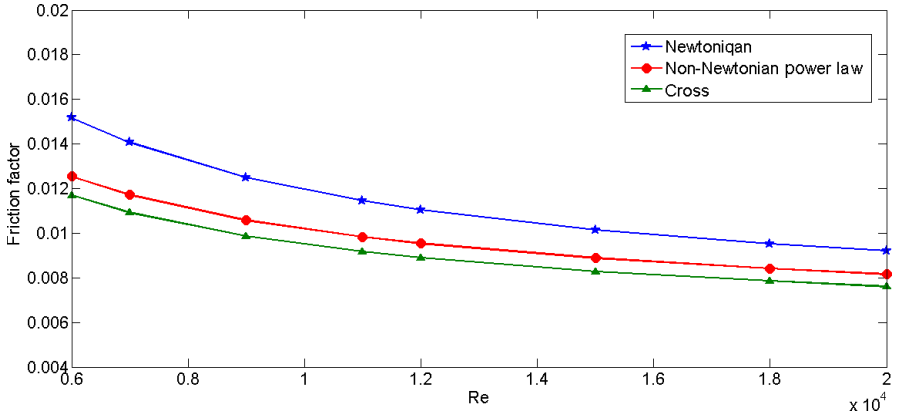

FIGURE 12 Turbulent flow friction factor in different Reynolds number

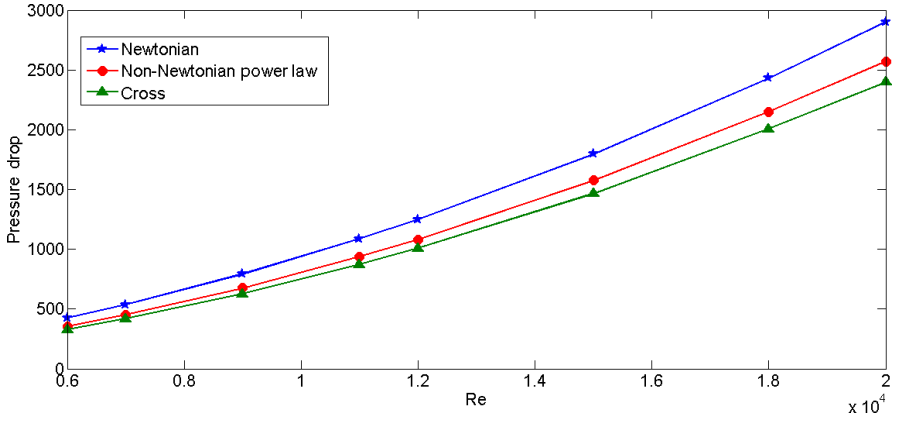

FIGURE 13 Turbulent flow pressure drop in different Reynolds number

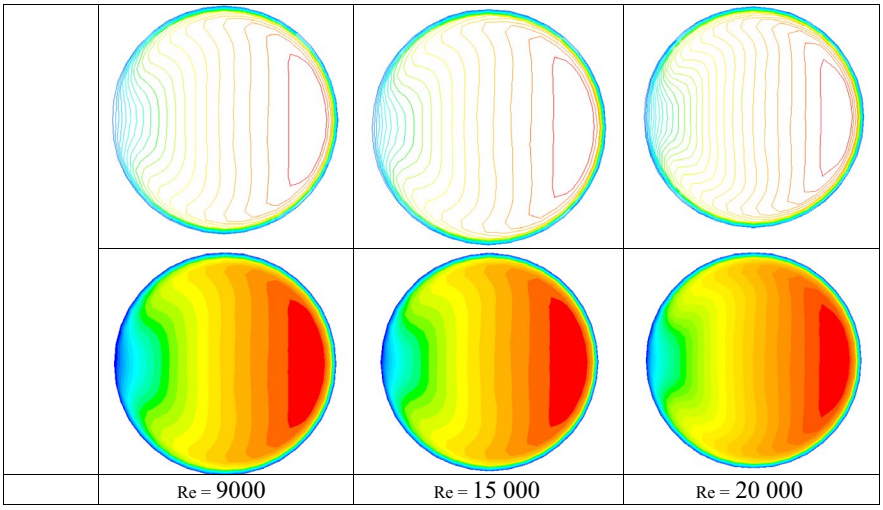

FIGURE 15 Distribution of velocity connectors in turbulent flow

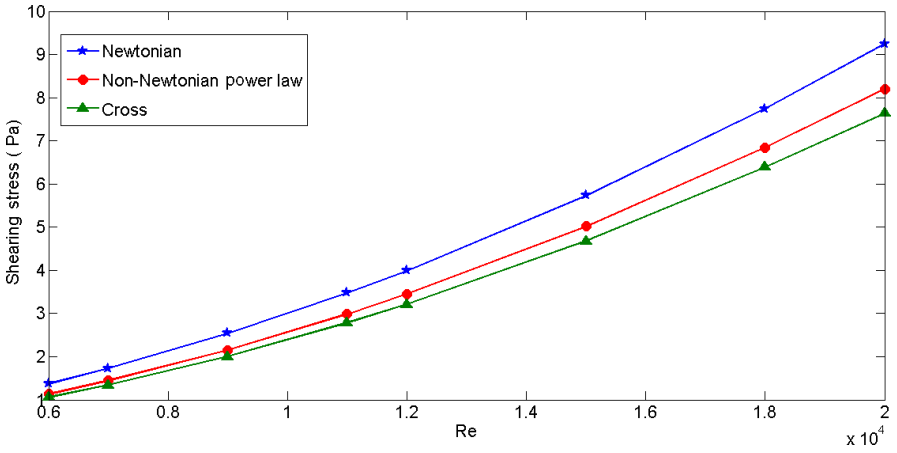

FIGURE 14 Turbulent flow shear stress in different Reynolds number

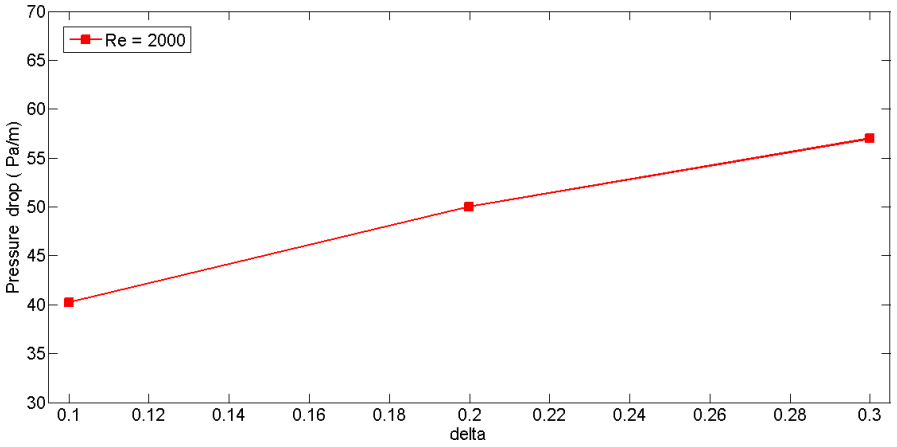

FIGURE 16 Pressure drop variations in different delta numbers

and shear stress of the wall increase. Increasing the wall shear stress and friction coefficient will increase the pressure drop inside the pipe. Therefore, it is observed that as the coil diameter decreases, the centrifugal force increases and this increases the friction coefficient and pressure drop of the tube.

In Figure 17, the friction coefficient graph is shown in terms of various values of delta for Reynolds number 2000. As described before, the friction coefficient has a positive relationship with the pressure drop, and it decreases by decreasing in curvature. Therefore, it is revealed that in terms of various amounts of delta, the friction coefficient increases as the curvature increases in a slow and turbulent flow. The pressure drop and friction coefficient are plotted for different steps. It can be seen that the change in coil step does not have any significant effect on them and the pressure drop and friction coefficient are almost constant because by changing the step, effective parameters on flow do not change, such as Reynolds number and secondary step.

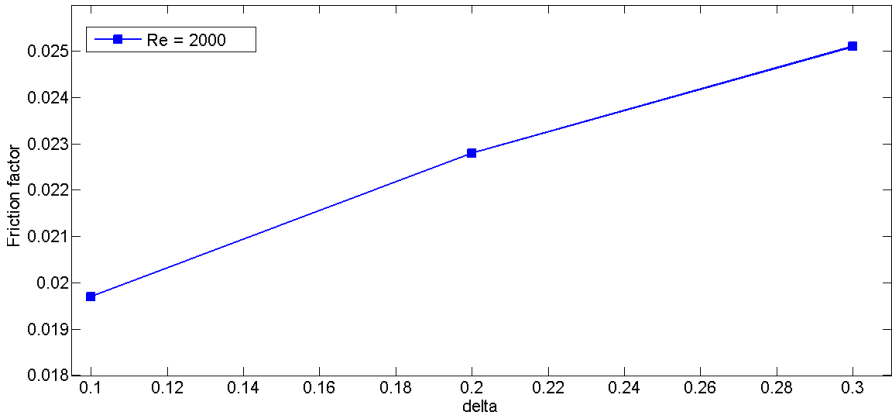

FIGURE 17 Friction factor variations in different delta numbers

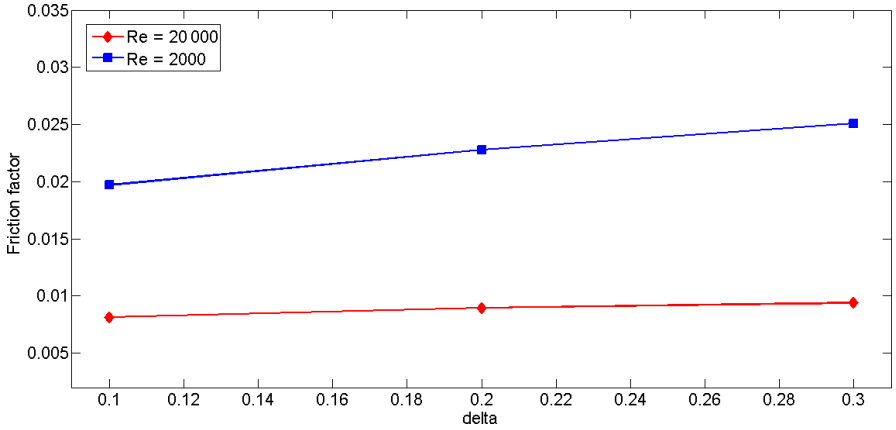

FIGURE 18 Friction factor variations in different delta numbers in two different Reynolds number

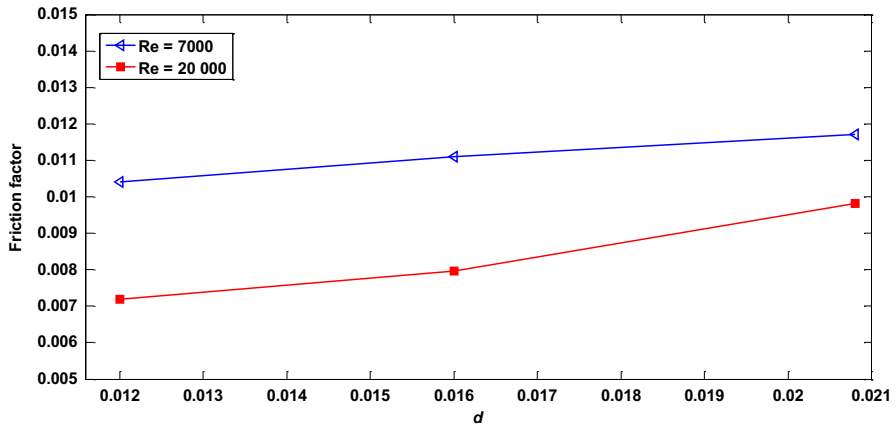

FIGURE 19 Effect of pipe diameter on the friction factor

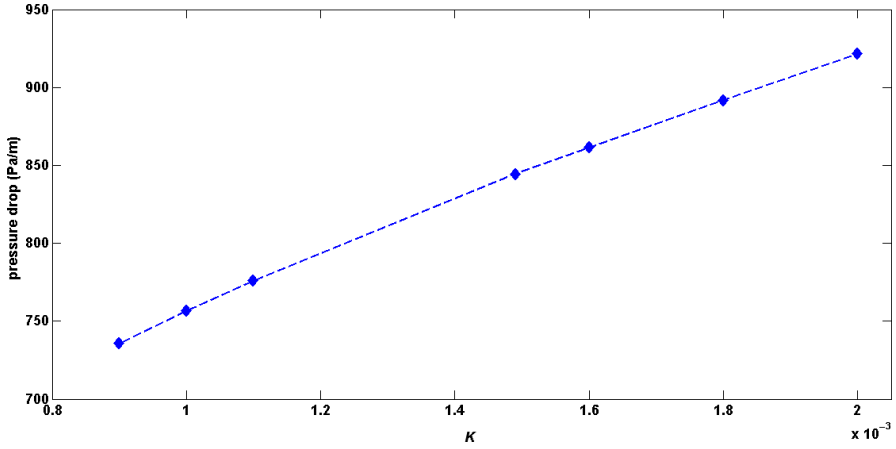

FIGURE 20 Pressure drop variations for different *K* values

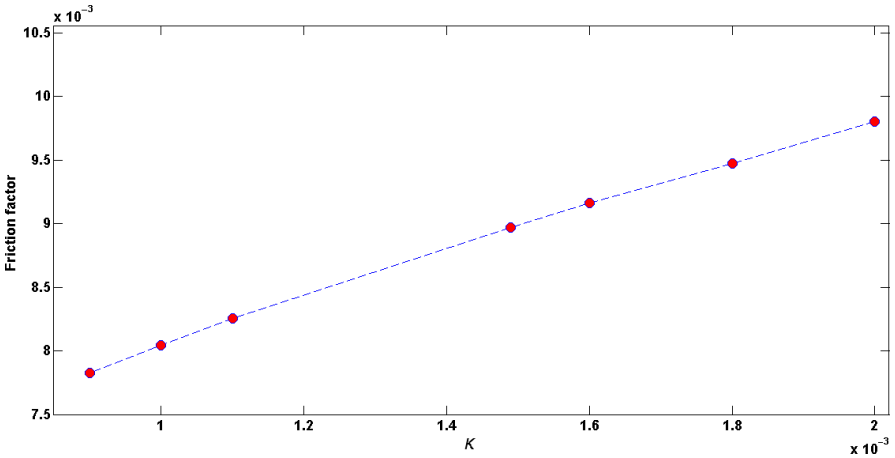

FIGURE 21 Friction factor variations for different *K* values

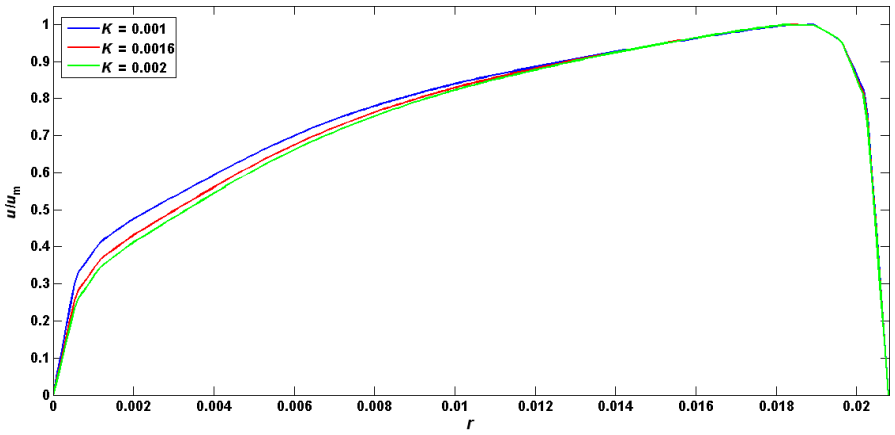

FIGURE 22 Velocity distributions for different *K* values

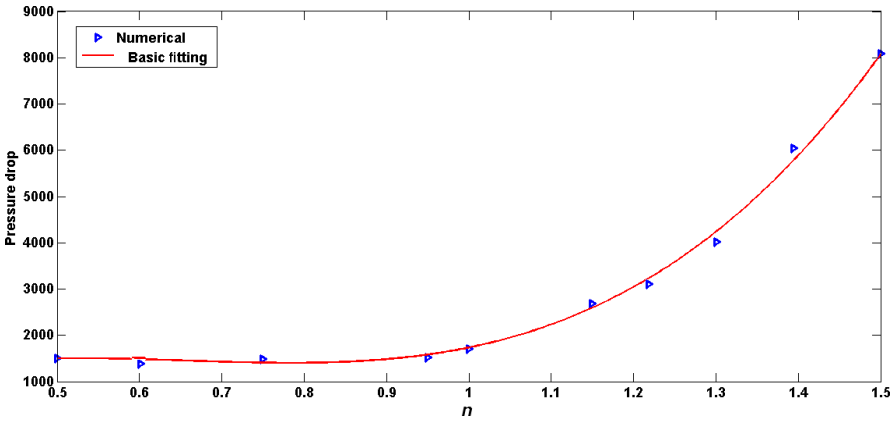

FIGURE 23 Pressure drop variations for different n values

In Figure 18, the friction coefficient graph is shown in terms of various values of delta for two Reynolds numbers. The curvature effect is plotted for two different Reynolds numbers, and in slow and turbulent flow, the coefficient friction increases as the curvature increases.

3.6.1 | Investigate the effect of pipe diameter change

To study the effect of pipe diameter change on the friction coefficient, three coils with diameters of 12, 16, and 20.8 mm were considered. The friction coefficient is calculated for two different Reynolds numbers. As seen, by increasing Reynolds number, the effect of diameter change on friction coefficient increases. In other words, for Reynolds number of 20 000, the percent of friction coefficient change by increasing the pipe diameter is 20% higher than it for Reynolds number of 7000, which is due to the existence of a secondary flow that is more effective for higher Reynolds numbers. It is shown in Figure 19.

3.6.2 | The K effect

In this case, n = 0.75, and the pressure drop graph is plotted for different *K* values. The *K* value is, in fact, the constant

value of viscosity, existence of the fluid viscosity, regardless the behavior of the material and acts as a constant coefficient in the shear stress equation, and its change causes changes in the kinematic viscosity of the material. In this section, the friction coefficient and pressure drop are plotted for a constant velocity with an increase in K value from 0.0009 to 0.002. Thereby, increasing the K value has a significant effect on the wall shear stress, which increases the friction coefficient and pressure drop inside the pipe. Also, increasing the K value will increase the thickness of boundary layer, as well as the friction coefficient. The increasing n will increase the thickness of the boundary layer, and this will increase the pressure drop and friction coefficient. It is plotted in Figure 20.

Increasing the K value has a significant effect on the wall shear stress, which increases the friction coefficient and pressure drop inside the pipe. In Figure 21, the impact of growing K value on various parameters is shown.

In Figure 22, the velocity profile at the coil outlet is plotted for three different K values. As shown in Figure 22, increasing the K value will increase the thickness of the boundary layer, as well as the friction coefficient.

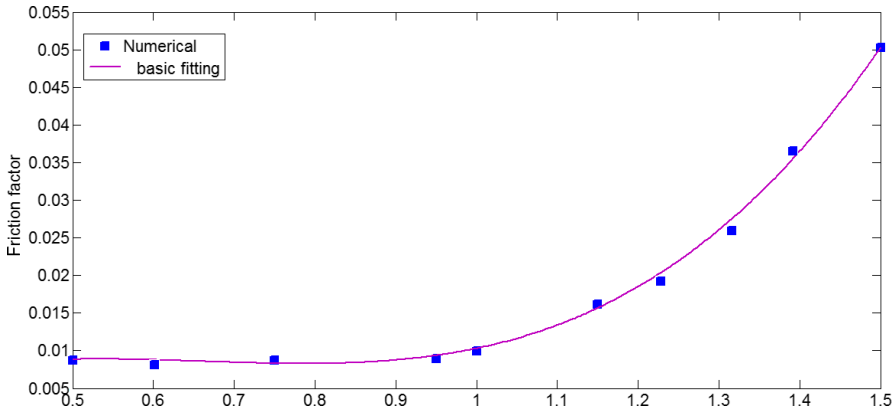

FIGURE 24 Friction factor variations for different n values

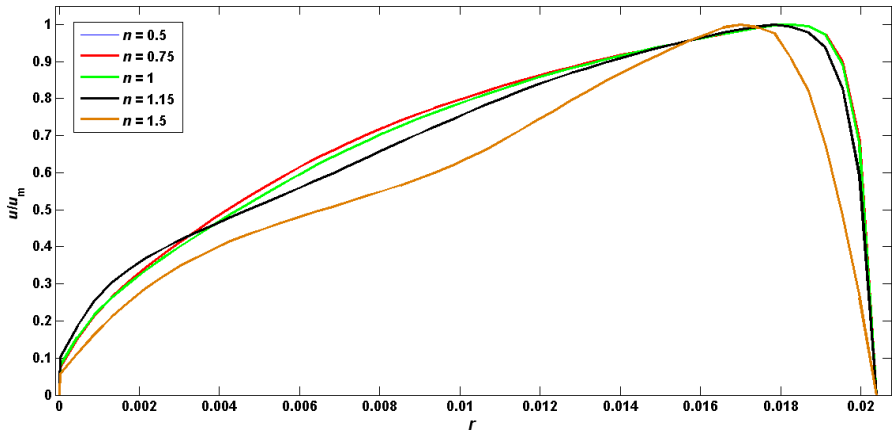

FIGURE 25 Velocity distributions in the outlet for different n values

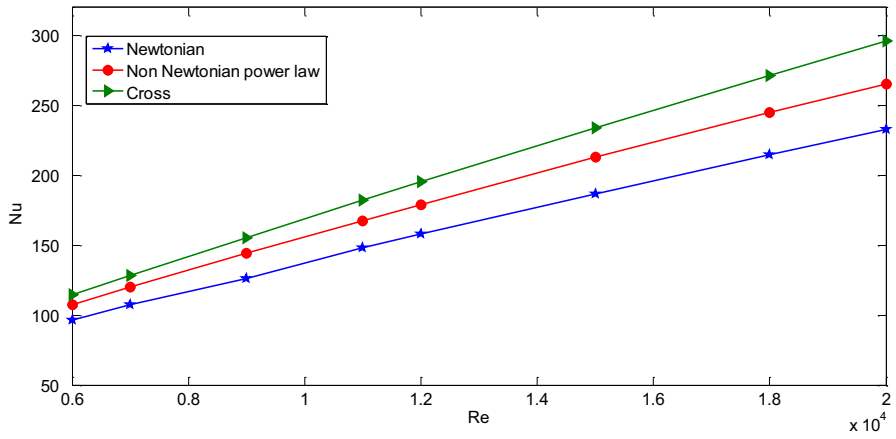

FIGURE 26 Nusselt number variations in different Reynolds for different models

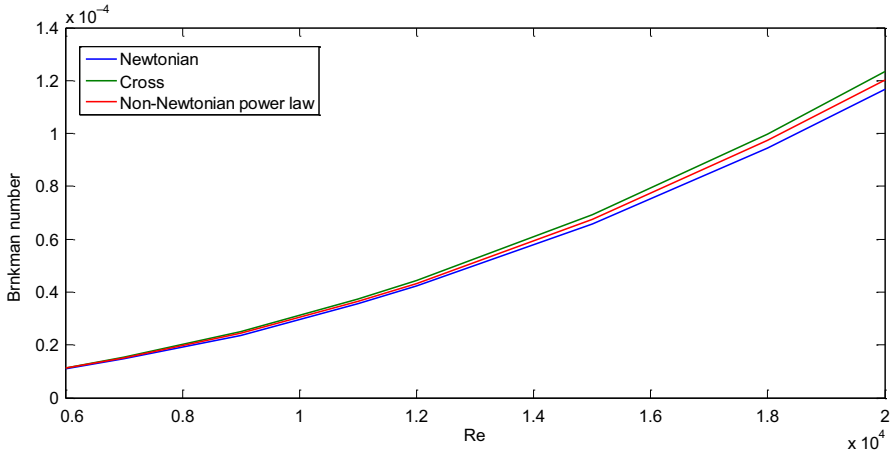

FIGURE 27 Brinkman number variations in different Reynolds for different models

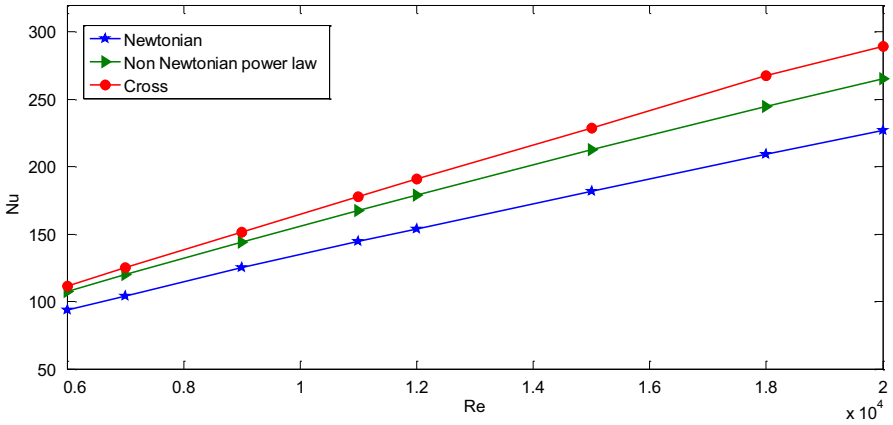

FIGURE 28 Nusselt number variations in different Reynolds for different models in the constant thermal flux state

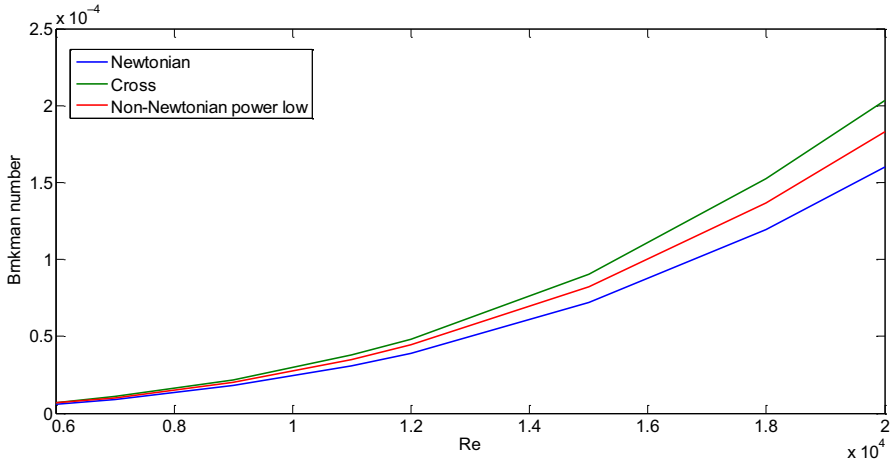

FIGURE 29 Brinkman number variations in different Reynolds for different models in the constant thermal flux state

3.6.3 | The effect of n

In this section, with the assumption that K value is constant, the pressure drop graph is plotted for different n values. As shown in Figure 23, for $n<1$, increasing the n will cause a very low change rate in pressure drop and friction coefficient, but for $n>1$, they are strongly affected by the n value so that by increasing n from 1 to 1.5, pressure drop and friction coefficient are about 4 times higher, while by increasing n from 0.5 to 1, this magnitude is about 30% for pressure drop.

The value of shear stress is related to the velocity gradient equation ($\tau=\mu_0\left(\frac{\partial u}{\partial y}\right)^n$), when $n>1$, increasing n will significantly increase the shear stress value. When $n<1$, the increase in the friction coefficient is very low. As shown in Figure 24, the thickness of the boundary layer does not change for $n<1$, and the effect of increasing n will increase the wall shear stress.

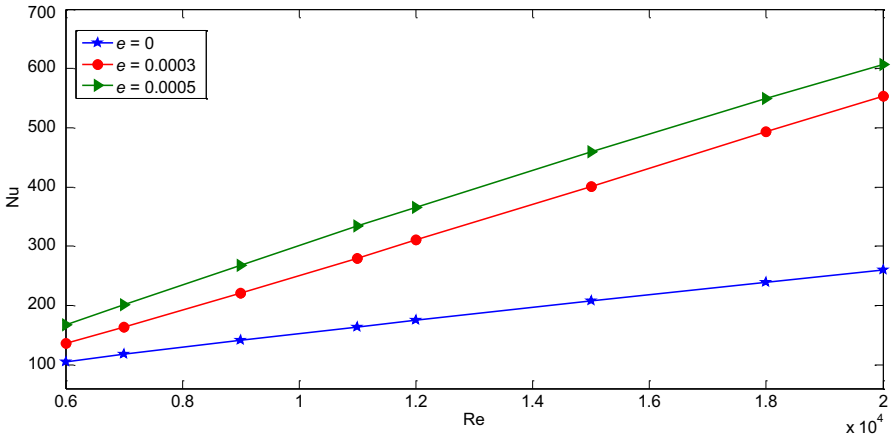

FIGURE 30 Nusselt number variations in different Reynolds for different roughness effects

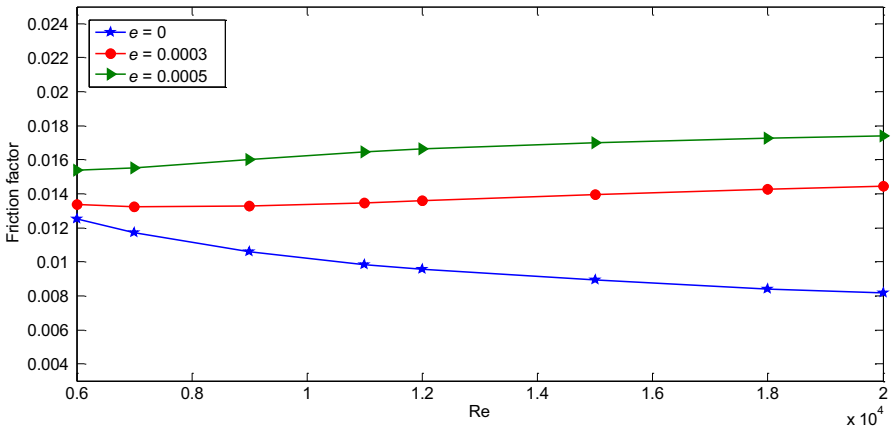

FIGURE 31 Friction factor variations in different Reynolds for different roughness effects

As shown in Figure 25, increasing n will increase the thickness of the boundary layer, and this will increase the pressure drop and friction coefficient.

3.7 | Examination of heat transfer characteristics

3.7.1 | Constant temperature state

In this part, the external temperature of the wall is $T = 340$ K; the fluid enters the spiral coil at a temperature of 290 K. Then, the Reynolds effects are examined on the Nusselt number, the external temperature of cross section, and other parameters in different models. As shown in Figure 26, increasing Reynolds number increases the Nusselt number. Increasing velocity near the wall will make turbulence, which increases the heat transfer coefficient.

The Brinkman number (Br) is obtained by $N_{\mathrm{Br}} = \frac{\mu U^2}{k(T_w - T_b)}$. According to this equation, factors such as velocity, wall temperature difference, and the mean flow velocity are dependents. As Reynolds number increases, although the wall and fluid temperature difference increase slightly, the effect of increasing velocity is much higher and causes Brinkman number to increase, as shown in Figure 27.

3.7.2 | Constant thermal flux state

In this part, the input thermal flux to the coil is considered to 200 kW/m^2, and the fluid flow enters the coil at a temperature of 290 K. By changing velocity, the Reynolds number of mean flow changes, causing a difference in the Nusselt number and wall temperature. Like the constant temperature state, increasing the velocity increases the turbulence near the wall, and it will increase the Nusselt number. It is shown in Figure 28.

In the constant flux state, the increase in velocity also increases the Brinkman number, and its difference with the constant temperature state is that the increase in Reynolds number decreases the differences between the average wall and fluid temperature. Therefore, the rise of the Brinkman number is much more in the constant flux state than in the constant temperature state. It is shown in Figure 29.

3.7.3 | The roughness effects

In this section, the roughness effects in turbulent flow are examined on increasing heat transfer and friction coefficient. To do it, the values of friction coefficient and Nusselt number are calculated in turbulent flow for different roughness.

As shown in Figures 30 and 31, increasing the amount of roughness will increase the friction coefficient due to the increase in turbulence. Also, by increasing turbulence inside the boundary layer, the heat transfer coefficient increases between the surface and the fluid that will increase the Nusselt number. It is worth to say that as the Reynolds number increases, the roughness effect is higher on the friction and heat transfer coefficients. For example, for Reynolds 6000, increasing the roughness from 0 to 0.0005, the increase in the friction and heat transfer coefficients is 30% and 70%, respectively. However, for Reynolds 20 000, the Nusselt number is three times higher, and the friction coefficient increases by 100%.

4 | CONCLUSION

The main conclusions which are obtained from this comprehensive study are as follows:

- In the study of slow flow, which is solved for the Reynolds range of 600-2500, increasing the Reynolds number decreases the friction coefficient.
- The non-Newtonian slow flow is solved with n = 0.75, and the friction coefficient is less than Newtonian fluid. It is observed that in slow flow, there is no significant difference between the results of cross and power law models.
- As the Reynolds increases near the wall, the velocity gradient increases, and this will increase the wall shear stress.
- The distribution of velocity profile has a slight difference at the pipe outlet for Reynolds 9000 and 20 000. In other words, the flow is constant in a developed region inside the spiral pipe.
- The investigation of pressure drop inside the pipe revealed that regarding the increase in Reynolds number, the friction coefficient decreases.
- In the flow inside the spiral pipe, due to the centrifugal force and the higher radius near the outlet surface, the velocity increases as it moves away from the coil center, and this causes that the shear stress in the outer wall is higher than the shear stress in the inner wall of the coil.
- Due to the various amounts of the delta, the friction coefficient increases as the curvature increases in slow and turbulent flow.
- The friction coefficient is calculated for two different Reynolds numbers. As seen, by increasing Reynolds number, the effect of diameter change on friction coefficient increases. In other words, for Reynolds number of 20 000, the percent of friction coefficient change by increasing the pipe diameter is 20% higher than it for Reynolds number of 7000, which is due to the existence of a secondary flow that is more effective in higher Reynolds numbers.
- Increasing the K value has a significant effect on the wall shear stress, which increases the friction coefficient and pressure drop inside the pipe. By changing velocity, the Reynolds number of mean flow changes, causing a difference in the Nusselt number and wall temperature.

NOMENCLATURE

$u(t)$	Turbulent velocity field
$\overline{u}$	Independent velocity from the selected time
$\overline{\eta}$	Mean quantity
λ	Thermal conductivity
ρ	Density
H	Coil height
D_c	Coil diameter
$\overline{\rho u_i' u_j'}$	Mean of density-weighted fluctuation
$\tau_{ij,\text{Turb}}$	Reynolds stress tensor

ORCID

Afshin Davarpanah https://orcid.org/0000-0002-3697-1808

REFERENCES

1. Aguirre A, Castillo E, Cruchaga M, Codina R, Baiges J. Stationary and time-dependent numerical approximation of the lid-driven cavity problem for power-law fluid flows at high Reynolds numbers using a stabilized finite element formulation of the VMS type. *J Nonnewton Fluid Mech*. 2018;257:22-43.
2. Davarpanah A, Mirshekari B. Sensitivity analysis of reservoir and rock properties during low salinity water injection. *Energy Rep*. 2019;5:1001-1009.
3. Davarpanah A, Shirmohammadi R, Mirshekari B, Aslani A. Analysis of hydraulic fracturing techniques: hybrid fuzzy approaches. *Arab J Geosci*. 2019;12:402.
4. Mehta D, Thota Radhakrishnan A, van Lier J, Clemens F. A wall boundary condition for the simulation of a turbulent non-Newtonian domestic slurry in pipes. *Water*. 2018;10:124.
5. Pico PD, Valdés JP, Ratkovich N, Pereyra E. Analysis of the drift flux in two-phase gas-liquid slug-flow along horizontal and inclined pipelines through experimental (non)-Newtonian and CFD Newtonian approaches. *J Fluid Flow Heat Mass Transf (JFFHMT)*. 2018;5:100-117.
6. Davarpanah A, Mirshekari B. Mathematical modeling of injectivity damage with oil droplets in the waste produced water re-injection of the linear flow. *Eur Phys J Plus*. 2019c;134:180.
7. Davarpanah A, Mirshekari B. Numerical simulation and laboratory evaluation of alkali–surfactant–polymer and foam flooding. *Int J Environ Sci Technol*. 2019. https://doi.org/10.1007/s13762-019-02438-9
8. Gijsen F, Allanic E, Van de Vosse F, Janssen J. The influence of the non-Newtonian properties of blood on the flow in large arteries: unsteady flow in a 90 curved tube. *J Biomech*. 1999;32:705-713.
9. Hassan M, Ellahi R, Zeeshan A, Bhatti MM. Analysis of natural convective flow of non-Newtonian fluid under the effects of

nanoparticles of different materials. *Proc Inst Mech Eng Part E: J Process Mech Eng*. 2019;233:643-652.
10. Jones J. Flow of a non-Newtonian liquid in a curved pipe. *Q J Mech Appl Math*. 1960;13:429-443.
11. RathnaS.Flow of a power law fluid in a curved pipe of circular cross-section. In: Proceedings of the conference on fluid mechanics; 1967:378.
12. Akbari OA, Safaei MR, Goodarzi M, et al. A modified two-phase mixture model of nanofluid flow and heat transfer in a 3-D curved microtube. *Adv Powder Technol*. 2016;27:2175-2185.
13. Davarpanah A, Mirshekari B. Experimental investigation and mathematical modeling of gas diffusivity by carbon dioxide and methane kinetic adsorption. *Ind Eng Chem Res*. 2019;58(27):12392-12400.
14. Davarpanah A, Mirshekari B. Experimental study of CO_2 solubility on the oil recovery enhancement of heavy oil reservoirs. *J Therm Anal Calorim*. 2019. https://doi.org/10.1007/s10973-019-08498-w
15. Jiang F, Wang K, Skote M, Wong TN, Duan F. Simulation of non-Newtonian oil-water core annular flow through return bends. *Heat Mass Transf*. 2018;54:37-48.
16. Sajadifar SA, Karimipour A, Toghraie D. Fluid flow and heat transfer of non-Newtonian nanofluid in a microtube considering slip velocity and temperature jump boundary conditions. *Eur J Mech B Fluids*. 2017;61:25-32.
17. Berger S, Talbot L, Yao L. Flow in curved pipes. *Annu Rev Fluid Mech*. 1983;15:461-512.
18. Canton J, Örlü R, Schlatter P. Characterisation of the steady, laminar incompressible flow in toroidal pipes covering the entire curvature range. *Int J Heat Fluid Flow*. 2017;66:95-107.
19. Dean WR. XVI. Note on the motion of fluid in a curved pipe. *London Edinburgh Dublin Philos Mag J Sci*. 1927;4:208-223.
20. Davarpanah A. A feasible visual investigation for associative foam > polymer injectivity performances in the oil recovery enhancement. *Eur Polymer J*. 2018;105:405-411.
21. Prabhanjan DG, Rennie TJ, Raghavan GV. Natural convection heat transfer from helical coiled tubes. *Int J Therm Sci*. 2004;43:359-365.
22. Ulker E, Korkut SO, Sorgun M. Computational analysis of turbulent flow through an eccentric annulus under different temperature conditions. *Int J Numer Meth Heat Fluid Flow*. 2018;28:2189-2207.
23. Zarei M, Davarpanah A, Mokhtarian N, Farahbod F. Integrated feasibility experimental investigation of hydrodynamic, geometrical and, operational characterization of methanol conversion to formaldehyde. *Energy Sources Part A: Recovery Utilization Environ Effects*. 2019;1-15.
24. Mehta D, Thota Radhakrishnan A, van Lier J, Clemens F. Sensitivity analysis of a wall boundary condition for the turbulent pipe flow of Herschel-Bulkley fluids. *Water*. 2019;11:19.
25. Valizadeh K, Davarpanah A. Design and construction of a micro-photo bioreactor in order to dairy wastewater treatment by micro-algae: parametric study. *Energy Sources Part A: Recovery Utilization Environ Effects*. 2019;1-14. https://doi.org/10.1080/15567036.2019.1588425
26. Acharya N, Sen M, Hsueh-Chia C. Heat transfer enhancement in coiled tubes by chaotic mixing. *Int J Heat Mass Transf*. 1992;35:2475-2489.
27. Jones SW, Thomas OM, Aref H. Chaotic advection by laminar flow in a twisted pipe. *J Fluid Mech*. 1989;209:335-357.
28. Rahul S. An experimental study for estimating heat transfer coefficient from coiled tube surfaces in cross-flow of air. In: Proceedings of the third ISHMT-ASME heat and mass transfer conference and fourth national heat and mass transfer conference, India, December, 1997; 1997.
29. Kalb C, Seader J. Heat and mass transfer phenomena for viscous flow in curved circular tubes. *Int J Heat Mass Transf*. 1972;15:801-817.
30. Rajasekaran S, Kubair V, Kuloor N. Secondary flow of non-Newtonian fluids in helical coils. *Indian J Technol*. 1966;4:33.
31. Raju KK, Rathna S. Heat transfer for the flow of a power-law fluid in a curved pipe. *J Indian Inst Sci*. 2013;52:34.
32. Nakayama A, Kuwahara F, Kokubo N, Ishida T, Ohara M. A numerical model for thermal systems with helically-coiled tubes and its experimental verification. *Heat Mass Transf*. 2002;38(4-5):389-398.
33. Jayakumar J, Mahajani S, Mandal J, Vijayan P, Bhoi R. Experimental and CFD estimation of heat transfer in helically coiled heat exchangers. *Chem Eng Res Des*. 2008;86:221-232.
34. Jayakumar J, Mahajani S, Mandal J, Iyer KN, Vijayan P. CFD analysis of single-phase flows inside helically coiled tubes. *Comput Chem Eng*. 2010;34:430-446.
35. Davarpanah A, Zarei M, Valizadeh K, Mirshekari B CFD design and simulation of ethylene dichloride (EDC) thermal cracking reactor. *Energy Sources Part A: Recovery Utilization Environ Effects*. 2019;41(13):1573-1587.
36. Shirmohammadi R, Gilani N. Effectiveness enhancement and performance evaluation of indirect-direct evaporative cooling system for a wide variety of climates. *Environmental Progress & Sustainable Energy*. 2018;38(3):e13032.
37. Davarpanah A, Mirshekari B. A mathematical model to evaluate the polymer flooding performances. *Energy Reports*. 2019;. https://doi.org/10.1016/j.egyr.2019.09.061
38. FLUENT A Fluent User's Guide, version 15. ANSYS Inc.
39. Pawar S, Sunnapwar VK. Experimental studies on heat transfer to Newtonian and non-Newtonian fluids in helical coils with laminar and turbulent flow. *Exp Thermal Fluid Sci*. 2013;44:792-804.
40. Kubair V. Pressure drop for liquid flow in helical coils. *Trans Indian Inst Chem Eng*. 1962;14:93-97.
41. Srinivasan P, Nandapurkar S, Holland F. Friction factors for coils. *Trans Inst Chem Eng*. 1970;48:T156.

How to cite this article: Valizadeh K, Farahbakhsh S, Bateni A, et al. A parametric study to simulate the non-Newtonian turbulent flow in spiral tubes. *Energy Sci Eng*. 2019;00:1–16. https://doi.org/10.1002/ese3.514